UCRL-15100

COMPTON SCATTERING

D. J. Botto
R. H. Pratt

May 1979

P.O. 9776403

UNIVERSITY OF PITTSBURGH
PITTSBURGH, PENNSYLVANIA

May 1979

Compton Scattering*

David J. Botto and R. H. Pratt

Department of Physics and Astronomy
University of Pittsburgh
Pittsburgh, Pennsylvania 15260

Abstract

The current status of Compton scattering, both experimental observations and the theoretical predictions, is examined. Classes of experiments are distinguished and the results obtained are summerized. The validity of the incoherent scattering function approximation and the impulse approximation is discussed. These simple theoretical approaches are compared with predictions of the nonrelativistic dipole formula of Gavrila and with the relativistic results of Whittingham. It is noted that the A^{-2} based

approximations fail to predict resonances and an infrared divergence, both of which have been observed. It appears that at present the various available theoretical approaches differ significantly in their predictions and that further and more systematic work is required.

Table of Contents

I. Introduction

Compton scattering[1,2] is the incoherent (inelastic) scattering of a photon by an electron which then recoils. Thus, if the electron is initially bound the Compton process is limited to the situation in which the atom is ionized (Compton scattering), rather than excited (Raman scattering) or left in its initial state (Rayleigh scattering). Here we restrict our attention to the situation in which one photon is scattered, not considering multiphoton or many electron effects or processes. As in all quantum electrodynamic processes, there are higher order radiative corrections to the basic calculation we are describing. The magnitude of such effects depends on the sensitivity (energy and angular resolution) of the experimental apparatus and the quantities observed -- for example, the extent to which radiation of two outgoing photons is excluded. (It is interesting to note that Compton scattering itself is a radiative correction to photoeffect, which must be calculated included in a calculation of quantum electrodynamic corrections to atomic photoeffect, particularly in the case of one soft outgoing photon.[3]) Photoeffect, scattering and pair production are the three processes primarily responsible for the attenuation of electromagnetic radiation in matter. Typically, for a given element the photoeffect dominates at low photon energies, scattering at intermediate energies, and pair production at high energies. In Fig. 1 we see that for the highest atomic numbers ($Z > 92$) scattering dominates the attenuation of radiation in matter only in the range from about .8 MeV to 4 MeV.[2] The range broadenes as Z decreases, becoming 0.1 MeV to 10 MeV for iron, while finally, for hydrogen, incoherent scattering dominates the total cross section from a few keV to 100 MeV.[2,4]

In Compton scattering from bound electrons the electron which scattered the photon is ejected from the atom; in the case that the ejection was from an inner shell of a high Z element shortly

after the ejection (10[-16] sec.) an outer electron makes a transition into the unfilled shell, thereby emitting characteristic radiation. (Filling of vacancies may also proceed through Auger transitions. For very large Z and for electronic transitions between the innermost shells, the Auger effect is less likely than the emission of X rays.[5]) In principle, one can observe the following aspects of Compton scattering: the energy (wavelength), momentum (scattering angle), and polarization of the scattered photon; the energy, momentum (scattering angle), and spin polarization of the ejected electron; and the energy, momentum, and polarization of the characteristic X ray. Although, in principle, all of the above quantities are measurable; in practice, only a few of the observables are measured. In this report we shall not consider observations of any of the polarization properties of the incident or final photons or ejected electrons. The most detailed type of experiment usually performed measures the energy and direction of the scattered photon in coincidence with the characteristic X ray emitted during the filling of the vacancy, thereby recording from which shell the electron was ejected. Such measurements usually involve inner shells of high Z ($Z > 47$) elements at high photon energies. Another common class of experiments measures the energy and direction of the scattered photon without observing the ejected electron. This class of experiments has generally been performed on low Z ($Z < 30$) elements for incident photon energies several times the K shell binding energy of the scatterer. A third class of experiments measures only the direction of the scattered photon. In this case both Compton scattering and Raman scattering contribute to the measured process. The least detailed experimental arrangement only measures the attenuation of radiation in matter, including photoeffect, scattering, and pair production processes.

The most widely used theoretical treatments of Compton scattering are based on the impulse approximation and the

incoherent scattering factor approximation. The impulse approximation relates the momentum distribution of electrons in the scatterer to the energy spectrum and direction of the scattered radiation. By contrast, the incoherent scattering factor approximation is generally used to describe the class of experiments measuring only the direction of the scattered radiation.

Recently, resonances have been observed for the Compton scattering of low energy photons, photons whose initial energy is slightly greater than the K shell binding energy of the scatterer. These resonances, not predicted by the above mentioned theories, occur when the incident photon ω_1 ejects an electron from the K shell while an outer shell electron fills the K hole emitting a photon of energy $\omega_2 = E_K - E_2$ (where E_K, E_2 is the K shell, outer shell binding energy) in the process. This effect has been termed Resonant Raman scattering.

We begin in the following section (Sec. II) by discussing Compton scattering from free electrons, which one anticipates does serve as a high energy limit of scattering from bound electrons once binding energies are small in comparison with photon energies. The various theories for Compton scattering from bound electrons and the approximations needed in their derivation are discussed in Sec. III. In Sec. IV we review the nature of the available experimental results and the accuracy with which the theories agree with experiment. Resonant Raman scattering and other low energy Compton scattering effects are discussed in Sec. V. We summarize our understanding of this process in Sec. VI and indicate certain needs for further work.

II. Scattering from free electrons

In photon scattering from electrons, if the initial photon energy is very much greater than other energies involved in the scattering process, one anticipates that the process may be described as scattering from free stationary electrons. This description is easiest to understand, so we present it first.

When a photon is scattered from a free stationary electron, the electron acquires some energy and momentum from the photon, hence the final photon is shifted in energy (wavelength) from its initial value. Compton[6], by considering the relativistic equations for conservation of energy and momentum and assuming an initial stationary free electron, derived the shift in wavelength of the scattered photon

$$\Delta\lambda = \frac{h}{m c}\,(1 - \cos\theta), \qquad (1)$$

where θ is the angle at which the photon is scattered. The shift in wavelength of the scattered photon is completely determined by the scattering angle. This result predicts that at a given scattering angle only one wavelength will be observed.

Early experimenters[7] using X rays on metal foils observed that the scattered radiation was not a sharp line whose position was completely determined by the scattering angle as in Eq. (1), but rather that the line was shifted from the value given in Eq. (1) and that the line had a broad shape. These features, explained by Dullond,[8] result from the initial momentum distribution of the bound and conduction electrons.

Assuming the electron is free but moving, one can show that for small initial electron momenta the shift in wavelength is given by

$$\Delta\lambda \approx \frac{h}{m c}\,(1 - \cos\theta) - \frac{2\lambda \sin^{\theta}/2}{m c}\,p_z, \qquad (2)$$

where λ is the initial photon wavelength and p_z is the component of the initial momentum of the electron parallel to the initial photon.

The relativistic cross section $d\sigma/d\Omega$ for Compton scattering from a free electron was first calculated by Klein and Nishina and by Tamm,[9] to lowest order in α. The differential cross section for unpolarized electrons in the rest system of the incident electron is[10]

$$\frac{d\sigma}{d\Omega} = \frac{\alpha^2}{4m^2}\left(\frac{\omega_2}{\omega_1}\right)\left(\frac{\omega_2}{\omega_1}+\frac{\omega_1}{\omega_2}+4(\bar{\epsilon}_1\cdot\bar{\epsilon}_2)-2\right), \qquad (3)$$

where

$$\omega_2 = \frac{\omega_1}{1+(\omega_1/m)(1-\cos\theta)}, \qquad (4)$$

where ω_1 and ω_2 are the energies of the initial and scattered photons, respectively. In the low energy limit of $\omega_1 \to 0$ this reduces to the classical Thomson scattering formula

$$\left(\frac{d\sigma}{d\Omega}\right)_T = \frac{\alpha^2}{m^2}(\bar{\epsilon}_1\cdot\bar{\epsilon}_2).$$

As the scattering angle $\theta \to 0, \omega_2 \to \omega_1$ and we find the Thomson cross section to be valid for all energies in the forward direction.

Several experiments at very high energies (photons with energies over 0.1 GeV) have tested total and angular distribution cross sections of Compton scattering and found agreement with the Klein - Nishina result to an accuracy of 10 to 15%.[11-15] At such high energies radiative corrections to single Compton scattering and double Compton scattering must be accounted for. These effects have been calculated by Brown and Feynman,[16] Anders,[17] Mork,[18] and Ram and Wang.[19]

Expressions for the Compton scattering from a thermal distribution of free electrons have been given by Ribberfors[20] and Hamada and Nakamura.[21] These expressions are an evaluation of the effective Klein-Nishina cross sections of electrons in thermal

equilibrium at a given electron temperature. The plasma described is optically thin, in that the scattering from individual electrons is incoherent.

III. Compton scattering from bound electrons

A. Nonrelativistic Formalism

Since most theoretical work to date is based on nonrelativistic quantum mechanics and the general features are, in fact, included in such a nonrelativistic description, we first discuss the nonrelativistic treatment of Compton scattering from bound electrons.

Nonrelativistically, in semi-classical radiation theory (considering the interaction of the atom with the radiation as a perturbation), one replaces the momentum $\bar{p}$ in the Hamiltonian by $\bar{p}-e\bar{A}$. The interaction Hamiltonian then contains two distinct terms[22]

$$H = e^2\bar{A}^2/2m - e\bar{p}\cdot\bar{A}/m. \qquad (5)$$

In first order pertubation theory the $\bar{p}\cdot\bar{A}$ term describes the emission and absorption of photons. The $\bar{A}^2$ term in first order pertubation theory and the $\bar{p}\cdot\bar{A}$ term in second order pertubation theory describe the scattering of a photon.

The differential cross section for Compton scattering by a bound electron may be written[23]

$$d^3\sigma = r^2 \frac{\omega_2}{\omega_1} |M_{fi}|^2 d\omega_2 d\Omega d\Omega_e \ , \qquad (6)$$

where $r = e^2/m$ and M_{fi} is the matrix element of the process. In the nonrelativistic case including retardation M is of the Kramers - Heisenberg - Waller type,[24,25] given by

$$M = (\bar{\varepsilon}_1\cdot\bar{\varepsilon}_2)\langle f|e^{i(\bar{k}_1-\bar{k}_2)\cdot\bar{r}}|i\rangle - \sum_n \frac{\langle f|e^{-i\bar{k}_2\cdot\bar{r}}\,\bar{\varepsilon}_2\cdot\bar{p}|n\rangle\langle n|e^{i\bar{k}_1\cdot\bar{r}}\,\bar{\varepsilon}_1\cdot\bar{p}|i\rangle}{E_n - (E_1+\omega_1+i\eta)} - \sum_n \frac{\langle f|e^{i\bar{k}_1\cdot\bar{r}}\,\bar{\varepsilon}_1\cdot\bar{p}|n\rangle\langle n|e^{-i\bar{k}_2\cdot\bar{r}}\,\bar{\varepsilon}_2\cdot\bar{p}|i\rangle}{E_n - (E_1-\omega_2)}$$

where $\bar{k}_1$ and $\bar{k}_2$ are the momenta of the initial and final photons, and $\bar{\epsilon}_1, \bar{\epsilon}_2$ their respective polarizations; $\bar{p}$ is the asympotic momentum of the ejected electron; $\bar{p}$ and $\bar{k}_2$ refer to the solid angles $d\Omega_e$ and $d\Omega$, respectively. Subscript i denotes the initial atomic state (energy E_1) and f denotes the final state of the atom and ejected electron (energy E_2). The infinitesimal positive quantity η appearing in the denominator of the first sum prevents the occurance of an unphysical singularity when the initial photon excites the electron into an intermediate continuum state with energy $E_n = E_1 + \omega_1$. Energy conservation requires that

$$E_1 + \omega_1 = E_2 + \omega_2. \tag{8}$$

Momentum is not conserved in the process as described here, since momentum will also be transfered to the nucleus of the atom. Therefore the directions of the outgoing photon and electron are not uniquely determined by momentum conservation arguements. Their energies can vary continuously from zero to upper limits fixed by Eq. (8), in contrast to the sharp angular dependent values they have when the initial electron is taken to be free.

The expression for M_{fi} in Eq. (7) is exact, to lowest order in the fine structure constant α, within nonrelativistic quantum mechanics, for a hydrogenlike atom. In the case of a many electron atom, described within a central self-consistent field approximation (the atomic electrons and the ejected electron move in the same central field in the initial, intermediate, and final states), when the scattering involves a one-electron transition, the matrix element is again given by Eq. (7).[23]

B. Hydrogenlike Case

For the hydrogenlike case, expressing the sums over

intermediate states in terms of momentum space integrals involving the Green's function for the Coulomb field, Gavrila[23] obtained an analytic expression, in terms of generalized hypergeometric functions, for the matrix element given in Eq. (7) for K shell electrons. Gavrila and co-workers in a series of papers extended this work by giving expressions for the matrix element in the dipole approximation (for incident and final photon energies sufficiently small so that the exponentials in Eq. (7) can be replaced by 1) for scattering by both the K[26,27] and L[28,29] shells. In the dipole approximation, if the outgoing electron is not observed, and if the photon polarizations are not observed, the relavent cross section is

$$\left(\frac{d^2\sigma}{d\Omega\, d\omega_2}\right) = \left(C_{1j} + C_{2j}\cos^2\theta\right)/2\, E_j, \qquad (9)$$

where j refers to the subshell from which the electron was ejected. This yields the shape of the scattered spectrum for every scattering angle. A further integration will give the over-all spectral distribution of the photons scattered into all space

$$\left(\frac{d\sigma}{d\omega_2}\right) = 2\pi\, (C_{1j} + C_{2j}/3)/E_j.$$

The values of C_{1j} and C_{2j} have been tabulated in Ref. 26 and 27 for the K shell and in Ref. 29 for the L shell.

For the K shell Gavrila predicted that for small incident photon energies, where the dipole approximation is valid, the angular distribution is isotropic. In this regime the matrix element together with the cross section of Eq. (9) decrease as $1/\omega_2$ as ω_2 increases from zero. The decrease is monotonic up to the end of the spectrum.

For larger incident photon energies, the first term of Eq. (7) becomes more and more important. For not too small scattering angles, this term produces a maximum in the cross section $d^2\sigma/d\Omega d\omega_2$, near the Compton frequency for scattering by free electrons. This maximum moves toward lower frequencies as the

angle increases. This broad maximum, related to the momentum distribution of the scattering electrons, contrasts with the sharp behavior of the Klein - Nishina cross section where ω_2 is uniquely determined by the incident photon energy and scattering angle. The low energy end of the spectrum ($\omega_2 \rightarrow 0$) is not dominated by this broad maximum, but rather is dominated by a $1/\omega_2$ behavior. This is an aspect of the infrared divergence of quantum electrodynamics.[30] Between these two features there exists a plateau which is a result of the constructive interference between their matrix elements.

The L shell scattering also exhibits the low energy ($\omega_2 \rightarrow 0$) infrared divergence of the spectrum and the broad maximum near the Compton frequency for scattering by free electrons. But even in the dipole approximation, the spectrum for scattering from 2p electrons also exhibits a resonance. This resonance occurs when the incident photon energy is larger than the K shell binding energy and the scattered photon has an energy of $\omega_2 = E_K - E_L$ corresponding to a bound-bound transition. At this energy the denominator of the second sum in Eq. (7) vanishes (in this approximation we have neglected the level widths of the electron states). If the numerator does not also vanish (the numerator does vanish for dipole scattering from the 2s subshell, essentially because the 1s - 2s transition is forbidden in dipole approximation), a resonance occurs. This resonance feature is not restricted to the 2p case, it will be present for scattering from other subshells.

The total intensity of photons scattered into a certain angle should be calculated by integrating Eq. (6) over both the outgoing electron angle and the outgoing photon energy. This should yield the analog of the Klein - Nishina cross section for bound electrons. However, because of the $1/\omega_2$ behavior of the matrix element as $\omega_2 \rightarrow 0$, $d\sigma/d\Omega$ does not exist. To accurately calculate this quantity, one must include the radiative corrections to the Compton process. One such correction is double Compton scattering,

where a second soft photon is also emitted during the scattering event. This demonstrates that when one wants to calculate $d\sigma/d\Omega$, the attenuation of a flux of photons passing through matter without observing the scattered photon energies and angles, the contribution of Compton scattering from bound electrons cannot be considered alone. To obtain such a cross section, one must also add the contribution of photoeffect, including the first-order radiative corrections to atomic photoeffect.[3]

C. The A^2 Approximation

Except for the work of Gavrila, all nonrelativistic treatments of Compton scattering by bound electrons which have been given so far are based on the $\bar{A}^2$ approximation of the matrix element M_{fi}, that is

$$M_{fi} \sim (\bar{\epsilon}_1 \cdot \bar{\epsilon}_2) \langle f | e^{i\bar{k}\cdot\bar{r}} | i \rangle. \qquad (10)$$

Eisenberger and Platzman[31] have argued that if ω_1 and ω_2 are much greater than $E_n - E_1$, then Eq. (7) may be approximated by

$$M_{fi} \sim \langle f | e^{i\bar{k}\cdot\bar{r}} | i \rangle \left(1 + \frac{p_2 p_1}{m} \frac{\omega_1 \omega_2}{\omega_1 \omega_2} \right), \qquad (11)$$

where all polarization factors have been dropped. The $\bar{p}\cdot\bar{A}$ contribution (the second part of Eq. (11)) is small in comparison to the $\bar{A}^2$ contribution in this limit. In fact, for stationary initial electrons $p_1=0$ and the contribution vanishes. However, at low energies the situation is reversed, since the $\bar{A}^2$ term of Eq. (7) vanishes in the dipole approximation, whereas the $\bar{p}\cdot\bar{A}$ term does not. In the limit $Z\to 0$ ($E_1\to 0$) Eq. (10) becomes exact and yields the nonrelativistic version of the Klein - Nishina cross section.

Using hydrogenlike wave functions for both the initial and final wave functions and assuming unpolarized radiation, Schnaidt[32] and Sujowski and Nagel[33] obtained the $\bar{A}^2$ approximation for the incoherent scattering of a photon into the energy interval $d\omega_2$ and solid angle $d\Omega$ by a K shell electron, where the final electron is represented by a continuum hydrogenlike state with a definite asympotic electron momentum, as

$$\frac{d^2\sigma}{d\Omega\, d\omega_2} = \frac{r^2}{2}\,(1+\cos^2\theta)\,\frac{256a^6\omega_2}{3\,\omega_1}\,\frac{q^2(a^2+p^2+3q^2)}{(a^2+(p+q)^2)^3(a^2+(p-q)^2)^3}$$

$$\times\,\frac{\exp\left(-\frac{2a}{p}\tan^{-1}\left(\frac{2pa}{a^2+p^2+q^2}\right)\right)}{1-\exp(-2\pi a/p)}, \qquad (12)$$

here $q=(\omega_2^2+\omega_1^2-2\omega_1\omega_2\cos\theta)^{1/2}$ is the momentum transfered to the atom, θ is the angle between $\bar{k}_1$ and $\bar{k}_2$, $\bar{p}$ is the momentum of the scattered electron, by energy conservation: $p^2/2 = \omega_1 - \omega_2 - a^2/2$, and $a = \alpha Z$.

For not too small scattering angles this result yields a scattered spectrum which exhibits a broad maximum centered about a line shifted from the free Compton frequency toward the energy of the incident photon. At smaller angles energy conservation cuts off the spectrum before it achieves its maximum. Since this is an $\bar{A}^2$ approximation the spectrum goes to zero as ω_2 goes to zero. By numerically integrating Eq. (12) over the magnitude of the electron momentum, they obtained a numerical result for $d\sigma/d\Omega$, which is a function only of $q'=q/a$. This cross section is zero at $q'=0$ and increases monotomically as q' increases approaching 1 for large q' ($q'>3$).

Shimizu et. al.[34] have derived an expression for the incoherent scattering of a photon into the solid angle $d\Omega$ by a K shell electron. They neglected transitions into excited discrete states, used a Coulomb wave function for the initial K shell electron and a plane wave for the ejected electron, and integrated

over all possible final states, and obtained

$$\frac{d\sigma_K}{d\Omega} = S \frac{d\sigma_F}{d\Omega},$$

$$S = \frac{32\sqrt{2}\ 137^2(E_{max}^{3/2} - E_{min}^{3/2})}{3\pi^2 Z^3 m^{3/2} c^3 (1+p^2/b^2)^4} \qquad (13)$$

where p is the initial momentum of the K shell electron ($p = (2mE_K)^{1/2}$), and b is Zh/a_0, where a_0 is the first Bohr radius. E_{max} and E_{min} can be estimated as

$$E_{max} = T + |E_K| + 2(T|E_K|)^{1/2}$$

$$E_{min} = T + |E_K| - 2(T|E_K|)^{1/2}, \qquad (14)$$

where $T = k\,A(1-\cos\theta)/(1+A(1-\cos\theta))$ and $A = k/mc^2$, and $d\sigma_F/d\Omega$ is the Klein - Nishina cross section. This result predicts a zero differential cross section at $\theta = 0$, and the cross section rises monotomically as θ increases.

The fact that the matrix element goes to zero as the scattering angle decreases is a general feature of all A^{-2} based approximations. The feature is a consequence of the orthogonality of the wave functions. At small scattering angles, the momentum transfer to the target electron tends to be small compared with their initial momentum, and there is a small probability that the atom will absorb enough energy to remove the target electron.

D. Incoherent Scattering Factor

All present theoretical tabulations[35-39] of the differential cross section $d\sigma/d\Omega$ of photons scattered from atoms are based upon the incoherent scattering function. Since the energy of the scattered photon is not observed, the differential cross section must include both excitation and ionization of the atom, and must be summed over all possible final states. In an independent

particle picture, the excitation or ionization involves one electron only, leaving the other electrons undisturbed. Thus the incoherent scattering function for an atom represents an average of the incoherent scattering functions for its separate electrons. The incoherent scattering approximation starts from Eq. (10) and makes the following further approximations:

(1) In the differential cross section

$$\frac{d^2\sigma}{d\Omega d\omega_2} = (\epsilon_1\cdot\epsilon_2)^2 \frac{\omega_2}{\omega_1} \sum_f \left|\langle f \sum_j e^{i(\bar{k}_1-\bar{k}_2)\cdot\bar{r}_j} |i\rangle\right|^2$$

$$X\delta(E_2+\omega_2-E_1-\omega_1), \qquad (15)$$

one replaces $(\bar{k}_1-\bar{k}_2)$ by $(\bar{k}_1-\omega_2^0\hat{k}_2)$ with $\hat{k}=\bar{k}/|k|$, and ω_2 by ω_2^0, where ω_2^0 is the mean of ω_2, then one can analytically integrate over ω_2, and usually one takes ω_1 or ω_2^0 as ω_2^0, where ω_2^0 corresponds to the (free) Compton frequency Eq.(4). This approximation is equivalent to asuming that the main contribution to the integral over ω_2 is from the region immediately surrounding the free Compton frequency.

(2) One assumes that the initial state and all possible final states form a complete set, and invokes the closure property. This ignores the fact that transitions from the initial state to occupied bound states are forbidden and not all continuum states are accessible due to the requirements of energy conservation. Then one obtains, on integration over scattered final photon energies ω_2,

$$\frac{d\sigma}{d\Omega} = \left(\frac{d\sigma}{d\Omega}\right) \frac{\omega_2^0}{\omega_1} \left(\sum_{i,j}\langle i|e^{i\bar{q}\cdot(\bar{r}_i-\bar{r}_j)}|i\rangle - F(q^2)^2\right), \qquad (16)$$

where $F(q^2)$ is the atomic form factor,

$$F(q^2) = \sum_n \langle i|e^{i\bar{q}\cdot\bar{r}}|i\rangle, \qquad (17)$$

and $\bar{q}=\bar{k}_1-\bar{k}_2$. (Note that in the $\bar{A}^2$ approximation, unlike the more exact infrared divergent full calculation, $d\sigma/d\Omega$ does exist.)

The incoherent scattering function is equal to zero at $\theta = 0$, due to the orthogonality of the wave functions. As the scattering angle increases the incoherent scattering function increases, becoming one for large momentum transfers. Eq. (16) has been evaluated using various types of wave functions (Herman-Skillman, Hartree-Fock, configuration interaction, etc.). The values obtained by the different evaluations vary by several per cent.

E. Impulse Approximation

The most commonly used theory to describe the spectral distribution of photons scattered from an atom $d^2\sigma/d\Omega\, d\omega_2$ is the impulse approximation. This theory depends upon the assumption that the energy transfered to the electron is large, so that electron binding energies can be neglected.

The case of a photon scattering from a free stationary electron was discussed in Sec. II. In this process the energy of the scattered photon is completely determined by the scattering angle and incident photon energy Eq. (4). If the electron is free but not stationary, the resulting cross section is given as[30]

$$\frac{d\sigma}{d\Omega} = \frac{r^2}{4\gamma^2(1-\beta\cos\alpha)^3}\left(\frac{\omega_2}{\omega_1}\right)\left(\frac{\omega_1}{\omega_2} + \frac{\omega_2}{\omega_1} - 2 + 4(\bar{\epsilon}_1\cdot\bar{\epsilon}_2)\right), \qquad (18)$$

where

$$\frac{\omega_2}{\omega_1} = \frac{1-\beta\cos\alpha}{1+\omega_1/m(1-\cos\theta)-\beta\cos\alpha'}. \qquad (19)$$

The angles α and α' are the angles between the incident electron and the incident and outgoing photon, respectively, and

$$|p| = \beta\gamma m, \qquad \gamma = \frac{1}{\sqrt{1-\beta^2}}$$

The angle ϕ is the angle between the planes formed by $\bar{k}_1, \bar{p}$ and $\bar{k}_1$,

$\bar{k}_2$. The angle α' can be expressed in terms of α, θ, ϕ:

$$\cos\alpha' = \cos\alpha\cos\theta + \sin\alpha\sin\theta\cos\phi.$$

If the electron does not have a single well defined momentum, but rather a momentum distribution as in the case of a bound electron, the scattered photon energy will not be a single frequency at a given scattering angle. The momentum distribution of the scattering electrons will produce a distribution of frequencies at each scattering angle.

By semiclassical arguements DuMond[8] related the spectral distribution of the scattered radiation to the momentum distribution of the bound electrons. His results were rederived and refined within the framework of quantum mechanics by Eisenberger and Platzman[31] and by Kilby.[40] The impulse approximation follows from the $\tilde{A}^2$ approximation and further assumes that the scattered electrons are free (but moving) during the entire collision process.[41] Before the collision let the electron have momentum p_1 and after the collision p_2. Then

$$E_1 = p_1^2/2$$
$$E_2 = p_2^2/2.$$

Conservation of momentum for this free electron case gives

$$\bar{p}_2 = \bar{p}_1 + \bar{k} \; ; \quad p_2^2 = p_1^2 + 2\bar{k}\cdot\bar{p} + k^2$$

and the delta function in Eq. (15) becomes

$$\delta((2\bar{k}\cdot\bar{p} + k^2 - \omega)/2) = \delta(k(\bar{k}\cdot\bar{p}/k - (\omega/k - k/2))).$$

Within the impulse approximation the final state is taken to be a plane wave

$$|f\rangle = e^{i\bar{p}\cdot\bar{r}}.$$

The momentum space bound state wave function is the Fourier transform of the corresponding position space function so that

$$X_1(\bar{p}_1) = (2\pi)^{-3/2}\int e^{-i\bar{p}\cdot\bar{r}} \quad \psi_1(r)\, d^3 r$$

and the sum over final states is

$$\sum_f \rightarrow \int (2\pi)^{-3} \quad d^3 p_2.$$

Choosing $\bar{k}$ to lie in the z direction and using momentum conservation

$$\sum_f |\langle f| e^{i\bar{k}\cdot\bar{r}} \quad |i\rangle|^2 \quad \delta(E_2 - E_1 - \omega_1 + \omega_2)$$

$$= \int d^3 p_2 \, |(2\pi)^{-3/2} \int d^3 r \, e^{i\bar{p}\cdot\bar{r}} \quad \psi_1(r)|^2 \, \delta(k(p_{1Z} - (\omega/k - k/2)). \tag{20}$$

Defining $q = \omega/k - k/2$. Eq. (20) reduces to

$$\int d^3 p_2 |X_1 \quad (p_1)|^2 \, \delta \quad (k(p_{1Z} - q)). \tag{21}$$

Noting that for ω_1 , θ and ω_2 fixed, k is fixed as well, it follows that the integral over $d^3 p_2$ is equivalent to an integration over $d^3 p_1$. Making use of the properties of the delta function Eq. (21) reduces to

$$\int\int_{-\infty}^{\infty} |X_1(p_{1x}, p_{1y}, q)|^2 dp_{1x}\, dp_{1y}$$

which is equivalent to an integration over the plane in momentum space p_{1Z}. For a momentum density which is spherically symmetric, it is convient to rewrite Eq. (21) in cylindrical coordinates where

$$J(q) = 2\pi \int_{(q)}^{\infty} |\psi_1 \quad (p_1)|^2 \, p_1 dp_1. \tag{22}$$

This becomes the result for the Compton profile in the impulse approximation

$$\frac{d^2\sigma}{d\Omega d\omega_2} = \left(\frac{d\sigma}{d\Omega}\right)_T \frac{r^2}{k} \frac{\omega_2}{\omega_1} J(q). \tag{23}$$

The impulse approximation is equivalent to a photon scattering inelastically from a free electron gas with a spherically symmetric momentum distribution where both energy and momentum are conserved

during the collision. The momentum density for any particular momentum in the free electron gas is obtained from the square of the Fourier transform of the initial bound state radial wave function. The energy-momentum conservation relations determine that for an incident photon with energy ω_1 scattering at any fixed $\bar{k}$, contributions to the scattering from electrons with momentum $\bar{p}$ can occur only if the projection of $\bar{p}$ on the scattering vector $\bar{k}$ equals q. This can occur if $|\bar{p}|$ is greater than or equal to q. The Compton profile is the projection of the electron momentum distribution onto the scattering vector, the one-dimensional momentum distribution function. The integration of Eq. (23) over ω_2 will yield a quanity which is comparable with the incoherent scattering factor. We have not found any discussion of this point.

In a simple description of photons scattering from a metal foil, the Compton profile J(q) is the sum of two distinct components. A broad background due to the core electrons. And, if the conduction electrons are treated as free in which all states below the Fermi momentum are occupied and all those above it are empty. the Compton profile is the projection of this distribution (a uniform sphere) onto a diameter. a parabola. Thus the profile for the foil is the sum of the two contributions. The area under each component curve is proportional to the number of electrons of that type. Realistically. the conduction electrons are not strictly free and hence their contribution to the profile will not be a simple inverted parabola.

Much of the work on Compton profiles has concentrated on using more accurate bound state wave functions in the calculation. For a good discussion of Compton profiles see the book Compton Scattering by B. Williams[42] and the review articles by Cooper.[22,43] In particular. profiles have been calculated using Hartree-Fock wave functions[44]. relativistic Hartree-Fock wave functions[45]. correlated wave functions.[46,47] and renormalized free atom models.[48] Such calculations yield results differing from each other by as much as 20%. but the basic validity of using such wave

functions in a nonrelativistic single particle formalism is an open question.

Although the impulse approximation is usually used to describe photon scattering from an atom, expressions have been given for scattering from certain individual subshells, in particular for scattering from the K shell of a hydrogenlike atom

$$\frac{d^2\sigma_K}{d\Omega d\omega_2} = \frac{1}{2} r^2 (1+\cos^2\theta) \frac{\omega_2}{\omega_1} \frac{8}{3\pi} \frac{a^6}{k} (a^2+q^2)^{-3}, \qquad (24)$$

Various investigators[31,49] have examined the effects of representing the ejected electron by a plane wave instead of a hydrogenlike continuum wave. These investigators have begun with Eq. (15), represented the final electron by a continuum Coulomb wave where $E_2 = p_2^2/2$. The sum over final states is replaced by an integral over the momentum of the outgoing electron. This quanity is then averaged over the directions of the electron momentum. Dividing by the Thomson cross section and the ratio of photon energies, they obtain an expression for the "exact" Compton profile. For weak binding and high incident photon energies the two results are similar ($\omega_1 - 100E_B$). As the scattering energy decreases the agreement worsenes. In many cases, using Coulomb wave functions rather than the plane wave for the continuum, secondary maxima occur which have been related to nodes in the bound state momentum wave function. However, for Coulomb wave functions such secondary maxima are too small to be observed in the sum of cross section profiles over all subshells in an atom.

F. Relativistic Approaches

For the most part, attempts at relativistic calculations of the Compton cross sections have involved evaluating the A^{-2} matrix element of Eq. (10),[50-53] the incoherent scattering function, and

the impulse approximation using relativistic wave functions. It is not clear whether such an evaluation is justified. (Such calculations rely on the fact that the nonrelativistic $\bar{p}\cdot\bar{A}$ term of the matrix element is small at high energy, but this need no longer be the case in the relativistic domain where $\bar{p}$ is not small.) Schumacher[52] has extended the work of Randles[50] obtaining an expression for $d^2\sigma/d\Omega\, d\omega_2$ for all s-subshells of the atom. This is an $\bar{A}^2$ approximation evaluated using relativistic Coulomb wave functions for the initial and final electron. He displayed results for incident photons of energy 662 keV scattering from lead into intermediate angles. To account for the shielding of the nuclear charge, effective charge numbers were used for the L_I, M_I, and N_I subshells; no shielding corrections were used for the K shell. His results for the energy spectra begin at very small values at $\omega_2 = 0$, have a maximum at energies slightly greater than the energy for scattering by free electrons, and drop abruptly to zero at $\omega_2 = \omega_1 - E_B$, where E_B is the binding energy of the electron. The shift of the maximum relative to the energy for free electrons decreases with increasing principal number. The curves obtained for the L_I, M_I, and N_I subshells have local minima close to the Compton maximum. These minima are related to the structure of the s-wave functions.

Pradoux et. al.[53]have evaluated the $\bar{A}^2$ approximation using a Coulomb K shell wave function for the initial electron and a Coulomb partial-wave series for the final electron for a variety of Z's at intermediate scattering angles and for ω_1=60 and 662 keV. For the low Z (Z=32) calculation at high energy, the maximum of the spectrum is shifted from the free Compton energy toward lower energies, for high Z (Z=82) at high energy the maximum is shifted toward higher energies.

A more consistent relativistic treatment would involve the evaluation of the second order S matrix. In the Furry picture[54], Compton scattering is described by the second order S matrix element

$$S_{fi} = S_{fi}^{(a)} + S_{fi}^{(e)}. \qquad (25)$$

where

$$S_{fi}^{(a)} = \frac{\alpha}{8\pi^2}(\omega_1\omega_2)^{-1/2}\int\int d^4x'd^4x\{\psi_f(x')\gamma\cdot\varepsilon_2^* e^{ik_2x'} S(x',x)\gamma\cdot\varepsilon_1 e^{-ik_1x}\psi_1(x)\}.$$

and

$$S_{fi}^{(e)} = S_{fi}^{(a)}\{k_2 <-> -k_1, \varepsilon_2^* <-> \varepsilon_1\},$$

are the amplitudes which correspond to the absorption of the incident photon before emission of the final photon and to the emission of the final photon prior to the absorption of the incident photon, respectively.[55] $S(x',x)$ is the electron propagator in the external field. Brown et. al.[56] developed a method of solution based upon defining, for a time independent external field,

$$F^{(a)} = \int d^4x\, S(x',x)\gamma\cdot\varepsilon_1 e^{-ik_1x}\psi_1(x). \qquad (27)$$

The amplitude $F^{(a)}$ satisfies the inhomogeneous Dirac equation

$$(H - k_1 - E_1) F^{(a)} = -\gamma\cdot\varepsilon_1 e^{-ik_1x}\psi_1(x),$$

and

$$S = -\frac{\alpha}{2\pi}(\omega_1\omega_2)^{-1/2}\int d^3x'\psi_2^+(x')\alpha\cdot\varepsilon_2 e^{ik_2x'} F^{(a)}(x'). \qquad (28)$$

By expanding the amplitude $F^{(a)}(x')$ and the final electron state in their respective partial wave series and the final photon in its multipole series, the matrix element may be written as an infinite sum of radial integrals over the product of radial wave functions and spherical Bessel functions. Brown et. al. applied this method to the calculation of Rayleigh scattering, and it has since been further developed for Rayleigh scattering by Johnson and Feiock[57] and Kissel and Pratt.[58]

Henry[59] has attempted to apply these methods to Compton scattering. He analytically performed the summation over hydrogenic intermediate states and performed the final radial integrations numerically to obtain the differential cross section

$d\sigma_K/d\Omega$. He compared his results to calculations of the incoherent scattering factor for the K shell of lead by scaling his hydrogenic results by $q'=q/\alpha Z$ (q is the momentum transfer, see Ref. 33).

Whittingham[60] performed a Coulombic numerical evaluation of S following the approach of Brown et. al. He completed a set of calculations for the doubly differential cross section $d^2\sigma_K/d\Omega\, d\omega_2$ of the K shell of lead at 662 keV. The energy spectrum, which he calculated, was shifted by 10% from the free Compton energy toward higher photon energies for scattering at 60°, This shift was angle dependent. It was toward lower energies at larger angles. The lowest scattered photon energy which he considered was 100 keV, which was within the region of least accuracy in his calculation. In this region his results did not exhibit a rise in the energy spectra as ω_2 decreased. To obtain the differential cross section $d\sigma_K/d\Omega$, he extrapolated his results to the $\omega_2 = 0$ region and numerically integrated over ω_2. His calculated cross section ratio $d\sigma_K/d\sigma_F$ is significantly larger than incoherent scattering function calculations.

Wittwer[61] performed numerical calculations of $d^2\sigma_K/d\Omega d\omega_2$ for gold at 145 and 320 keV and tin at 145 keV. He did not follow the approach of Brown in that he numerically performed the sums over intermediate states and neglected binding effects in the intermediate states. He also truncated his calculation at l=2 for both the initial and final photon multipole series, where l is the angular momentum of the multipole operator. His results, claimed to be accurate within 12%, displayed a striking infrared divergence. The effect dominates his calculation of gold at 145 keV.

Owen[62] has performed an analytic calculation of the differential cross section and Compton profile by ignoring the effects of the external field after the initial photon-electron interaction. In this approximation, the free electron propagator is used instead of the Coulomb propagator in Eq. (26) and the final

electron is represented by plane waves. He then solved the second order S matrix and obtained expressions for both the doubly and singly differential cross sections, $d^2\sigma/d\Omega\, d\omega_2$ and $d\sigma/d\Omega$, in terms of the upper and lower radial components of the initial electron wave function. These results reduce to the Klein-Nishina cross section for scattering from free stationary electrons.

C. Comparison of theoretical approaches

Both Tseng et. al.[25] and Pradoux et. al.[53] have made comparisons between the various theoretical results for K shell electrons in a hydrogenlike atom. Tseng et. al. compared the nonrelativistic $\bar{A}^2$ formula of Schnaidt,[32] Eq. (12), and the nonrelativistic dipole $\bar{p}\cdot\bar{A}$ formula of Gavrila[26] and the hydrogenic impulse approximation, Eq. (24), with the numerical results of Whittingham.[60] In Figs. 2-4 we display their comparison for the doubly differential cross section $d^2\sigma_K/d\Omega d\,\omega_2$. We see that in general the $\bar{A}^2$ approximation and the impulse approximation are relatively close to each other at all displayed scattering angles and energies. But that the $\bar{p}\cdot\bar{A}$ results of Gavrila and the relativistic results of Whittingham differ strongly with each other and with the two $\bar{A}^2$ based approximations. In Fig. 5 we display the singly differential cross section $d\sigma/d\Omega$. (where to obtain a meaningful result, the integral over the $\bar{p}\cdot\bar{A}$ term in Gavrila's work was evaluated using a low energy cutoff). At small scattering angles we see that calculations utilizing relativistic wave functions are nonzero at $\theta = 0$. At larger scattering angles the discripences cannot be so easily classified. All calculations, except the nonrelativistic $\bar{A}^2$ and impulse, disagree with each other. They also concluded that in the calculation of total cross sections, the $\bar{A}^2$ approximation gives very bad predictions for photon scattering near the K edge and

gives results accurate to less than 10% for photon energies larger than 20 times the K shell binding energy.

Pradoux's work also shows significant differences between relativistic and nonrelativistic calculations. They compared K shell results of theirs with those of Schnaidt, Gavrila, Whittingham, and Schumacher. They reported that the position of the maximum of the spectra agree in relativistic calculations of Whittingham, Pradoux, and Schumacher. This position does not agree with the nonrelativistic calculations of Gavrila and Schnaidt. In all their cases the full width at half maximum for all nonrelativistic calculations are larger than those for relativistic calculations. Whittingham's results are consistently larger than all the other calculations.

It appears that at this point that the various theoretical approaches differ significantly and that one cannot have any confidence in any of these approaches.

IV Experiments and comparison to theoretical work

The recent interest in Compton measurements, going back to the 1960's, has resulted from technical improvements in computers and detectors. The experimental efforts have been concentrated mainly in two directions. One is to study the detailed profile J(q) of the Compton line and its relation to the electronic momentum distribution of the scatterer. In this type of experiment a monochromatic, collimated beam of photons is scattered from the sample and a energy (wavelength) analysis of the beam scattered through a fixed angle is carried out. This class of experiments has usually been performed on lower Z elements, where it has been believed that the nonrelativistic A^2 approximation which underlies the analysis is justified.

The other main experimental direction tries to isolate the contribution to the Compton cross section $d\sigma/d\Omega$ from individual atomic shells by using favorible experimental setups. The principle of such experiments is always related to the emission of an X ray following the ejection of a bound electron. The X ray, characteristic of the atomic energy level, is emitted shortly after the interaction. When this X ray is observed in concidence with the scattered photon, the incoherent scattering event can be associated with scattering from electrons in a particular shell. This is generally the K shell of medium to high Z elements, due to their higher characteristic energies, these characteristic X rays are easier to detect.

There are also a limited number of experiments measuring the doubly differential cross section from the K shell separately, or focussing on the total atom cross section rather than J(q), as well as, measurements of the singly differential cross section $d\sigma/d\Omega$ from total atoms. We shall briefly comment upon each of these areas of experimentation in this section, beginning with the doubly differential cross section $d^2\sigma/d\Omega\, d\omega_2$ in A and B, and the singly

differential cross section in C. In each section we examine both the total atom and shell studies.

A. Measurement of J(q)

There have been numerous measurements of the Compton profile J(q)[42], usually on the lower Z elements (Z<36) at incident photon energies between two and 3000 times the K shell binding energy. The most commonly used incident energies are 17.4, 59.54, and 159 keV. Measurements of J(q) require substantial unfolding of the raw experimental data. The results J(q) are typically displayed graphically, thereby easily showing the general features: a sharp peak due to the valence or conduction electrons superimposed upon a broad peak due to the inner shell (core) electrons. These measurements on gases, liquids, solids, crystals, and molecules easily show the environmental effects upon the outer or conduction electron momentum densities. The main thrust of this work has been to determine the wave functions which yield J(q) agreeing with experiments best.

B. Measurement of $d^2\sigma/d\Omega d\omega_2$

Using coincidence measurement techniques the energy spectra of Compton scattering from the K shell of atoms has been reported by Spitale[63], Pradoux et. al.[53], and Kane.[64] Spitale performed measurements on gold (Z=79), holmium (Z=67), tin (Z=50), and iron (Z=26) at incident photon energies of 145, 320, and 662 keV. Spitale's measurements showed a scattered peak superimposed on a continuum which appeared to diverge at the low end of the spectrum. The scattered peak was narrower than would be expected from the

bound state electron motion, the peak width reached a maximum near Z=50 and then decreased with increasing atomic number. His measurements disagreed with Wittwer's predictions on the behavior of the infrared divergence as a function of scattering angle, and also on the behavior of the broadened peak. Pradoux et. al. have measured the energy spectrum from Cu (Z=29), Ge (Z=32), and Mo (Z=42) at incident energies of 60 and 662 keV. Within the experimental accuracy, their measurements agree with his relativistic evaluation of the $\tilde{A}^{-2}$ approximation; predictions for the shift of the maximum and the full width at half maximum.

Schumacher et. al.[52,65] have measured and reported directly the differential cross section $d^2\sigma/d\Omega\, d\omega_2$ for 662 keV photons incident on lead and incident photons at 279 keV on copper, tin, and lead. For the scattering of 662 keV photons, they report - the differential cross section begins at very small values of $\omega_2 \sim 100$ keV, have a maximum at energies slightly larger than the energy for scattering by free electrons, and drop to zero abruptly at $\omega_2 = \omega_1 - E_B$ with E_B the binding energy of the electron. There are abrupt drops in the differential cross section at 573.6 and 646 keV corresponding to the disappearence of the contributions of the K and L shells, respectively. At 279 keV they compared their experimentally measured differential cross section to an impulse approximation based upon Coulomb wave functions of an effective charge to represent screening and a nonrelativistic $\tilde{A}^{-2}$ calculation. They observed that at the high energy end of the spectrum there is a discrepency of 1.5 in the case of copper and a factor of 4 in the case of lead, which they attribute to a deviation of the $\tilde{A}^{-2}$ approximation from second order pertubation theory.

C. Measurements of $d\sigma/d\Omega$

Most recent work[33,34,66-79] on the angular distribution of

scattered photons has involved coincidence measurements which identify from which shell the electron was ejected. Due to the energy cutoff of the experimental equipment, these experiments do not measure the divergent part of the energy spectrum. Experiments which isolate the the contribution to the compton line by individual atomic shells show the effects of binding upon the scattered cross section. At the large scattering angles, where the energy transfer to the K electrons is large compared to their initial energy, the cross section for scattering approaches the Compton cross section for scattering by free electrons with velocities approaching the initial velocity of the scattered electron.

Another expected effect of binding of target electrons is a lowering of the cross section in the forward direction, in comparison to that for free electrons. At small scattering angles, the momentum transfer to the target electron tends to be small compared with their initial momentum, and there is a small probability that the atom will absorb enough energy to remove the target electron.

In Tables I - IV, we give most of the published values of the differential K shell cross section ratio $d\sigma_K/d\sigma_F$, where $d\sigma_F$ is the free electron (Klein-Nishina) cross section. Table I shows the differential cross section ratios for an incident photon of 279 keV. At this energy there is no overlap between the experimental groups, each group has performed their work on a different set of elements. It is interesting to point out that the results obtained by Pingot for Ta (Z=73) are approximately half of the values obtained by Murty et. al. for W (Z=74). The experimental results have been compared to evaluations of Eqs. (12) and (13), as well as, to averages over angle of Eq. (19), where the electron is assumed to have a momentum whose magnitude is given by the binding energy. All of these theoretical approaches differ significantly from the measured values. Table II shows the cross section ratios for an incident photon of energy 320 keV. The results of the two

experiments are in very good agreement, but it should be noted that the results came from the same laboratory.

The cross section ratio $d\sigma_K/d\sigma_F$ at ω_1=662 keV is by far the most widely studied. All this work clearly supports the general trends noted by early workers: the lowering of the cross section ratio at small angles and as the angle increases the cross section ratio increases monotonically. But the absolute values for a given cross section ratio vary by as much as 40%. The measured values are greater than K shell incoherent scattering factors at small angles and larger than the averaged (over angle) Klein-Nishina for large angles. Pingot's measured values are consistently lower than those of other experimenters, although the general trends are comparable. These results also strongly disagree with evaluations of Eq. (12), (13), and (19). For the case of lead the experimental results have been compared to the work of Whittingham. Whittingham's predictions lie within the experimental bars of Shmizu et. al., Motz and Missoni, and East and Lewis; but lie above the error bars given by Sujowski and Nagel and Pingot.

For completeness in Table IV we give the recently published results for the cross section ratio at the incident photon energy of 1120 keV. Here the agreement between theory and experiment is also very bad. Studies of the L shell scattering ratios are very limited. Murty et. al.[78] have published data for 279 keV photons scattering from the L shell of thorium (Z=90). We can see some trends if we compare $d\sigma_K/d\sigma_F$ to $d\sigma_L/d\sigma_F$ at the same atomic charge and incident photon energy. For small angles $d\sigma_L/d\sigma_F > d\sigma_K/d\sigma_F$ and for $\theta \geq 100^\circ$ $d\sigma_L/d\sigma_F < d\sigma_K/d\sigma_F$. For this energy ($\omega_1 \sim 2.5\ E_K$ and $\omega_1 \sim 14\ E_L$, where E_K and E_L are the binding energies of the K and L shells, respectively) binding effects are expected to be large.

There has been much less recent work on the singly differential cross section of total atoms. Hubbell et. al.[39] compare the incoherent scattering factors with available measurements and conclude that agreement is within the experimental error bars except for Al at ω_1=8.05 keV and Pb at ω_1=280 and 662

keV at low momentum transfers where the theoretical values are systematically higher. This contrasts with the K shell measurements where the measured values are systematically higher.

V Low energy Compton scattering and the Resonant Raman effect

Contrary to calculations based upon the of $\bar{A}^2$ approximation, which predict that the scattering cross section goes monotomically to zero as the incident photon energy goes to zero, Sparks[80] observed that when the incident photon energy is near an atomic absorption edge a resonant enhancement in the scattering cross section occurs. This phenomena has since been termed the Resonant Raman scattering. This effect - that the spectrum of the scattered X rays is resonantly enhanced at a final photon energy corresponding to a transition between bound states (for example, K shell photoeffect followed by a L-K transition) - can be explained in a single particle model. The incoming photon excites a K electron to a P like continuum state, an L shell electron drops into the K hole emitting a photon of frequency $\omega_2(=\omega_1-(E_L+E_K))$ thereby leaving a hole in the L shell.

Gavrila and Tugulea[29], independent of the experiments, had found this Resonant Raman feature in their analytic calculation of Compton scattering. Extending the work of Gavrila and co-workers[26-29], they showed that light scattered by the 2p state of atomic hydrogen displayed the following features: (1) A peak displaced from the exciting frequency by the 2p binding energy. This peak corresponds to the Resonant Raman peak discovered by Sparks; (2) a low frequency - infrared - divergence; (3) a plateau between these two features which is a result of constructive interference between their matrix elements.

The resonant effect as well as the constructive interference plateau has since been observed by other workers.[81-85] Although the onset of the infrared divergence has yet to be confirmed at these incident photon energies. The experimental spectral densities are in qualitative, but not quantitative, agreement with Gavrila's calculations. This quantitative discrepency, presumably,

reflects the differences between hydrogen and a solid. Sannett[83] has gone beyond Gavrila's work and has evaluated the relavent matrix element in a dipole approximation using a single Slater determinant constructed from the one-electron orbitals of Clementi.[86] This result when scaled to the maximum of the experimental curve yields excellent qualitative agreement with their measured curve for Ni which is near resonance, but is much worse for elements off resonance.

This resonant effect should not be limited to a final L shell hole, but the effect should be present for any shell hole (L,M,N,etc.). The M shell hole has been observed by Kodre and Shafroth.[84] Similar resonances can be observed not just near the K edge, but near other edges.

VI Conclusions

Compton scattering is commonly described within the nonrelativistic $\bar{A}^2$ single particle frozen core formalism. Investigators have evaluated these $\bar{A}^2$ approximations using Hartree-Fock, relativistic, and correlated wave functions. However, the validity of the basic nonrelativistic $\bar{A}^2$ approximation has never been established.

A correct nonrelativistic description of Compton scattering in a single particle model includes both an $\bar{A}^2$ and a $\bar{p}\cdot\bar{A}$ term. This description predicts that the cross section $d\sigma/d\omega_2$ diverges as $\omega_2 \to 0$. This effect results from the infrared divergence of quantum electrodynamics, and will be present in any more complete theory. The divergence has been observed experimentally and is more prominant at small scattering angles. Calculations limited to the $\bar{A}^2$ approximation do not show the effect. In consequence of this divergence the value obtained for the measured singly differential cross section $d\sigma/d\Omega$ is dependent upon the energy resolution of the measuring apparatus. This fact may account for Hubbell's claim that $\bar{A}^2$ based incoherent scattering factors agree within experimental error for large scattering angles, but disagree at small angles (where the divergent $\bar{p}\cdot\bar{A}$ contribution to the matrix element remains dominant for more of the observed spectrum).

Although Hubbell claims good agreement for photon scattering from the total atom, the agreement between theory and experiment is much worse for the differential cross section ratios $d\sigma_K/d\sigma_F$ and $d\sigma_L/d\sigma_F$. The majority of these experiments have been performed at high incident photon energies where relativistic effects may be important.

For incident photon energies above the K edge of the scattering element, a resonant enhancement of the differential cross section has been observed for scattered photon energies resulting from bound - bound transitions. This effect, which has

been called Resonant Raman scattering, is not predicted by the simpler $\bar{A}^2$ based approximations. Qualitative agreement between experiments and theory have been achieved using a single particle $\bar{p}\cdot\bar{A}$ description of the process. Although a description giving quantitative agreement will probably require a many body description of the process.

A single particle relativistic calculation of Compton scattering would probably resolve the descrepency between theory and experiment for the differential cross section ratios $d\sigma_K/d\sigma_F$ and $d\sigma_L/d\sigma_F$. It would also, most likely, improve the agreement between theory and experiment for the singly differential cross section $d\sigma/d\Omega$ at small scattering angles (where the infrared divergence becomes important). At low photon energies such a calculation would probably give qualitative agreement near the Resonant Raman peaks.

But a single particle calculation, whether relativistic or nonrelativistic, cannot be expected to resolve discrepencies due to many bod, effects, such as; scattering from the conduction band electrons in a metal. Many body effects are most important near the peak in a Compton spectrum, as in the Resonant Raman regime.

References

1. A. Sommerfeld, Atombau and Spektrallinien, (Viewez, Braunsheriez, 1939), Vol. 2, Ch. 8.
2. R. D. Evans, Encyclopedia of Physics, ed. S. Flugge (Springer-Verlag, Berlin, 1958), Vol. 34, p. 218.
3. J. McEnnan and M. Gavrila, Phys. Rev. A 15, 1537 (1977).
4. J. H. Hubbel and Wm. J. Veigle, NBS Tech. note 901 (1976).
5. H. A. Bethe and E. E. Salpeter, Quantum Mechanics of one- and two- Electron Atoms, (Plenum, New York, 1977), p. 295.
6. A. H. Compton, Phys. Rev. 21, 483 (1923).
7. P. A. Ross and P. Kirkpatrick, Phys. Rev. 45, 134 (1934); 45, 223 (1934); 46, 668 (1934).
8. J. W. M. DuMond, Rev. Mod. Phys. 5, 19 (1933).
9. O. Klein and Y. Nishina, Z. Physik 52, 853 (1929); I. Tamm, ibid. 62, 545 (1930).
10. J. D. Bjorken and S. D. Drell, Relativistic Quantum Mechanics, (McGraw-Hill, New York, 1964), Sec. 7.7.
11. F. H. Coensgen, University of California Radiation Lab. Rept. UCRL-2413 (1953).
12. L. V. Kurnosova, L. A. Razorenov, and P. A. Cherenkov, Zh. Eskp. Teor. Fiz. 30, 690 (1956); JETP 3, 546 (1956).
13. J. D. Anderson, R. W. Kenney, and C. A. McDonald, Jr., Phys. Rev. 102, 1626 (1956).
14. B. Gittelman, W. C. Barber, W. Selove, D. Tompkins, and F. Forman, Phys. Rev. 171, 1388 (1968).
15. A. T. Goshaw, T. Glanzman, L. R. Fortney, W. J. Robertson, and W. D. Walker, Phys. Rev. D 18, 1351 (1978). TR/78./
16. L. M. Brown and R. P. Feynman, Phys. Rev 85, 231 (1952).
17. T. B. Anders, Nuc. Phys. 87, 721 (1969).
18. K. J. Mork, Phys. Rev. A 4, 917 (1971): the coefficient of the $\ln|k|$ term should be $-\frac{5}{6}\pi^2$ in Eq.6.2 of this paper.
19. M. Ram and P. Y. Wang, Phys. Rev. Lett. 26, 476 (1971): 26,

1210 (E) (1971).

20. R. Ribberfors, J. Quant. Spectrose. Radiat. Transfer 16, 689 (1976).
21. T. Hamada and Y. Nakamura, Prog. Theor. Phys. 60, 1717 (1978).
22. M. Cooper, Adv. Phys. 20, 453 (1971).
23. M. Gavrila, Phys. Rev. A 6, 1348 (1972).
24. H. A. Kramers and W. Heisenberg, Z. Physik 31, 681 (1925); I. Waller, ibid. 51, 213 (1928); 58, 75 (1929).
25. H. K. Tseng, M. Gavrila, and R. H. Pratt, NBS Rept. no. 2 (1973) (unpublished).
26. M. Gavrila, Phys. Rev. A 6, 1360 (1972).
27. M. Gavrila, Rev. Roum. Phys. 19, 473 (1974).
28. A. Costescu and M. Gavrila, Rev. Roum. Phys. 18, 493 (1973).
29. M. Gavrila and M. N. Tugulea, Rev. Roum. Phys. 20, 209 (1975).
30. See, for example, J. M. Jauch and F. Rohrlich, The Theory of Photons and Electrons, (Addison-Wesley, Cambridge, Mass., 1955).
31. P. Eisenberger and P. M. Platzman, Phys. Rev. A 2, 415 (1970).
32. F. Schmidt, Ann. Physik 21, 89 (1934).
33. Z. Sujkowski and B. Nagel, Arkiv. Fysik 20, 323 (1961).
34. S. Shinizu, Y. Nakayama, and T. Mukoyama, Phys. Rev. 140, A806 (1965).
35. H. P. Hanson, F. Herman, J. D. Lea, and S. Skillman, Acta Cryst. 17, 1040 (1964).
36. D. T. Cromer, J. Chem. Phys. 50, 4857 (1969); Los Alamos Scientific Lab. Rept. LA4079 (1969).
37. E. Storm and H. I. Israel, Nuc. Data Tables A7, 565 (1970).
38. Wm. J. Veigle, Atomic Data 5, 51 (1973).
39. J. H. Hubbell, Wm. J. Veigle, E. A. Briggs, R. T. Brown, D. T. Cromer, and B. J. Howerton, J. Chem. Phys. Ref. Data 4, 471 (1975).
40. G. E. Kilby, Proc. Phys. Soc. 86, 1037 (1965).
41. L. B. Mendelsohn, and V. H. Smith, Jr., Compton Scattering, ed. B. Williams (McGraw Hill, New York, 1977), Ch. 5.

42. B. Williams, see other chapters of Ref. 41.

43. M. Cooper, Contemp. Phys. 18, 489 (1977).

44. F. Briggs, L. B. Mendelsohn, and J. B. Mann, Atomic Data and Nuclear Data Tables 16, 201 (1975).

45. F. Briggs, L. B. Mendelsohn, and J. B. Mann, Sandia Lab. Rept. 75-0636 (1976).

46. V. H. Smith, Jr. and R. E. Brown, Chem. Phys. Lett. 20, 424 (1973).

47. M. Maon and M. Cornille, J. Phys. B 6, 954 (1973).

48. T. Paakkari, K. F. Berggren, R. Ribberfors, and V. Halnen, Phys. Rev. B 14, 2301 (1976).

49. B. J. Block and L. B. Mendelsohn, Phys. Rev. A 9, 129 (1974).

50. J. Randles, Proc. Phys. Soc. A70, 337 (1957).

51. K. G. Standing and J. V. Jovanovich, Can. J. Phys. 40, 622 (1962).

52. H. Schumacher, Z. Physik 242, 444 (1971).

53. M. Pradoux, M. Meunier, M. Avon, and G. Roche, Phys. Rev. A 16, 2022 (1977).

54. W. H. Furry, Phys. Rev. 81, 115 (1951).

55. One can derive the nonrelativistic result Eq. (7) by starting from the exact relativistic matrix element for a bound electron and taking the nonrelativistic limit ignoring spins, see A. I. Akhiezer and V. B. Berestetskii, Quantum Electrodynamics, (Interscience, New York, 1965), Sec. 35.I.

56. G. E. Brown, R. E. Peierls, and J. B. Woodward, Proc. R. Soc. A 227, 51 (1954).

57. W. R. Johnson and F. D. Feiock, Phys. Rev. 168, 22 (1969).

58. L. Kissel and R. H. Pratt, Phys. Rev. Lett. 40, 387 (1978).

59. E. Henry, (Phd. thesis, unpublished, 1969).

60. I. B. Whittingham, J. Phys. A 4, 21 (1971).

61. L. Wittwer, (Phd. thesis, unpublished, 1972).

62. D. A. Owen, Phys. Rev. A 16, 1594 (1977); Phys. Lett. 69A, 177 (1978).

63. C. C. Spitale, Lawrence Livermore Lab. Rept. UCRL-51596

(1974).

64. P. N. Baba Prasad, G. Basaveraju and P. P. Kane, Phys. Rev. A 15, 1984 (1977).

65. P. Rullhusen and M. Schumacher, J. Phys. B 9, 2435 (1976).

66. D. Brini, E. Fuschini, N. T. Grimellini, and D. S. R. Murty, Nuovo Cimento 16, 727 (1960).

67. J. W. Motz and C. Missoni, Phys. Rev. 124, 1458 (1961).

68. J. Varma and M. A. Eswaram, Phys. Rev. 127, 1197 (1962).

69. L. V. East and E. R. Lewis, Physica 44, 595 (1969).

68. A. Ramalinga Reddy, V. Lakshminarayana, and S. Jnanananda, Ind. J. Pure Appl. Phys. 4, 371 (1966).

71. O. Pingot, Nuc. Phys. A119, 667 (1968); J. de Physique 32, 413 (1971).

72. S. N. Chintalapudi and K. Parthasaradhi Ind. J. Phys. 43, 492 (1969).

73. D. S. R. Murty, D. V. Krishna Reddy, and E. Narasimhacharyulu, Ind. J. Pure Appl. Phys. 9, 305 (1970); Physica 75, 394 (1974).

74. A. Ramalinga Reddy, V. Lakshminarayana, and S. Jnanananda, Proc. Phys. Soc. 91, 71 (1967).

75. O. Pingot, Nuc. Phys. A133, 334 (1969); J. de Physique 33, 189 (1972).

76. D. S. R. Murty, V. Govindareddy, and E. Narasimhacharyulu, J. Phys. A 6, 265 (1973).

77. D. S. R. Murty, V. Govinda Reddy, and C. Nageswara Rao, Physica 92C, 137 (1977); J. Phys. B 10, 47 (1977).

78. S. T. P. V. J. Swamy and D. S. R. Murty, Physica 84C, 289 (1976).

79. P. N. Baba Prasad and P. P. Kane, J. of Research NBS 78A, 461 (1974); Phys. Rev. A 15, 1976 (1977).

80. C. J. Sparks, Jr., Phys. Rev. Lett. 33, 262 (1974).

81. Y. B. Bannett, J. I. Gersten, N. Tzoar, and I. Freund, Phys. Rev. Lett. 36, 882 (1976).

82. P. Eisenberger, P. M. Platzman, and H. Winick,

Phys. Rev. Lett. 36, 623 (1976); Phys. Rev. B 13, 2377 (1976).

83. Y. B. Bannett, D. C. Rapaport, and I. Freund, Phys. Rev. A 16, 2011 (1977).

84. A. F. Kodre and S. M. Shafroth, Phys. Rev. A 19, 675 (1979).

85. J. H. Hall, K. A. Jamison, O. L. Weaver, and P. Richardson, Phys. Rev. A 19, 568 (1979).

86. E. Clementi, IBM J. Res. 9, 2 (1965).

Figure Captions

Fig. 1. Locus of equal atomic cross sections for Compton and photoeffect interactions ($\sigma = \tau$), and for Compton and pair-production interactions ($\sigma = \kappa$). The incident photon energy is $h\nu$, and Z is the atomic number of the atoms in the absorber. Compton collisions have larger cross sections than any other mode of interaction in the entire domain of medium energy photons marked "Compton effect dominant". (from Ref. 2).

Fig. 2 Comparison of the pure Coulomb K shell Compton scattering cross section $d^2\sigma/d\Omega d\omega_2$ for Z=82, ω_1 = 662 keV and $\theta = 0$ between the relativistic results of Whittingham (Ref. 60), of the $\bar{A}^2$ approximation of Schnaidt (Ref. 32), of the impulse approximation Eq. (24), and of the $\bar{A}^2$ together with the dipole $\bar{p}\cdot\bar{A}$ formula of Gavrila. The binding energy E_K is calculated nonrelativistically. The Compton energy is indicated by a straight line. (from Ref. 25).

Fig. 3. Same as Fig. 1 except $\theta = 60°$.

Fig. 4. Same as Fig. 1 except $\theta = 180°$.

Fig. 5. Comparison of the pure Coulomb K shell scattering cross section $d\sigma/d\Omega$ for Z=82, ω_1 = 662 (keV) between, the relativistic results of Whittingham and of various other approximations. Symbols NR and R refer to nonrelativistic and relativistic cases. (from Ref. 25)

TABLE I. Experimental cross section ratios $d\sigma_K/d\sigma_F$ for an incident photon energy of 279 keV. The reference from which the values were obtained is given next to the chemical symbol.

	$d\sigma_K/d\sigma_F$					
θ°	Ag (Ref. 75)	Sm (Ref. 75)	Ta (Ref. 75)	W (Ref. 76)	Au (Ref. 75)	Th (Ref. 77)
20	.158 ± .03	.161 ± .06	.189 ± .04		.206 ± .02	
30				.267 ± .04		.330 ± .04
50				.456 ± .06		.391 ± .015
55	.542 ± .04	.294 ± .08	.290 ± .04		.317 ± .03	
70				.689 ± .04		.571 ± .04
90	.844 ± .08	.550 ± .08	.358 ± .06		.378 ± .03	
105				.819 ± .04		.751 ± .05
125	1.039 ± .06	.691 ± .06	.487 ± .05	.94 ± .08	.426 ± .03	.908 ± .17
150						1.160 ± .04
160	1.076 ± .07	.740 ± .04	.502 ± .07		.449 ± .02	

TABLE II. Experimental cross section ratios $d\sigma_K/d\sigma_F$ for an incident photon energy of 320 keV. Otherwise the same as Table I.

	$d\sigma_K/d\sigma_F$					
θ°	Sm (Ref. 74)	Sm (Ref. 72)	Ta (Ref. 74)	Ta (Ref. 72)	Pb (Ref. 74)	Pb (Ref. 72)
45	.645 ± .097	.65 ± .10	.525 ± .079	.53 ± .08	.50 ± .075	.50 ± .08
60	.750 ± .113	.75 ± .11	.660 ± .099	.66 ± .1	.595 ± .089	.60 ± .1
90	.825 ± .124	.83 ± .13	.745 ± .112	.75 ± .11	.700 ± .105	.70 ± .11
110	.905 ± .136	.91 ± .14	.850 ± .128	.85 ± .13	.835 ± .125	.84 ± .13

TABLE III. Experimental cross section ratios for an incident photon energy of 662 keV. Otherwise the same as Table I.

$d\sigma_K/d\sigma_F$

θ°	Ag (Ref. 71)	Sn (Ref. 70)	Sm (Ref. 70)	Sm (Ref. 71)	Sm (Ref. 72)	Ta (Ref. 71)	Ta (Ref. 70)	Ta (Ref. 69)
20	.411 ± .06			.391 ± .08		.313 ± .07		.42 ± .15
30		.659 ± .07	.617 ± .09		.63 ± .09		.485 ± .05	
40								1.09 ± .11
45		.717 ± .08	.755 ± .11		.76 ± .12		.727 ± .08	
50								1.28 ± .1
55	.802 ± .06			.843 ± .07		.847 ± .06		
60		.882 ± .09	.915 ± .14		.92 ± .14		.921 ± .1	
70								1.33 ± .24
90	.949 ± .05	1.075 ± .11	1.160 ± .17	1.088 ± .06		1.191 ± .05	1.132 ± .12	
105								
125	.991 ± .05			1.070 ± .07		1.324 ± .06		
130		1.184 ± .13	1.375 ± .21				1.358 ± .14	
140								
160	1.015 ± .06			1.148 ± .07		1.410 ± .06		

(TABLE III continued)

Ta (Ref. 72)	Pt (Ref. 73)	Au (Ref. 69)	Au (Ref. 71)	Pb (Ref. 70)	Pb (Ref. 72)	Bi (Ref. 73)	Th (Ref. 73)
.49 ± .05		.31 ± .12	.335 ± .05		.52 ± .06		
	.522 ± .047			.515 ± .05		.471 ± .105	.453 ± .049
		.79 ± .09	.561 ± .04				
.73 ± .08				.715 ± .08	.72 ± .08		
	.857 ± .045	1.04 ± .1				.974 ± .086	.0843± .048
.92 ± .1			.743 ± .04	.863 ± .09	.86 ± .09		
	1.160 ± .098	1.10 ± .20				1.140 ± .193	1.120 ± .074
1.13 ± .12			.960 ± .04	1.289 ± .14	1.29 ± .14		
	1.380 ± .169					1.456 ± .318	1.487 ± .180
	1.660 ± .115		1.154 ± .04				
1.36 ± .14				1.542 ± .17	1.54 ± .17	1.725 ± .140	1.780 ± .086
			1.263 ± .04				
			1.335 ± .04				

TABLE IV. Experimental cross section ratios for an incident photon energy of 1120 keV. Otherwise the same as Table I.

	$d\sigma_K/d\sigma_F$				
θ	Sn (Ref. 79)	Ta (Ref. 79)	Au (Ref. 79)	Pb (Ref. 79)	Th (Ref. 79)
25	.71 ± .07		.63 ± .09		.40 ± .13
60	.86 ± .08		.81 ± .09	.86 ± .1	.91 ± .11
90	.94 ± .08		1.33 ± .12		1.36 ± .12
100			1.44 ± .15		1.20 ± .39
120		.91 ± .26	.98 ± .15		.93 ± .15

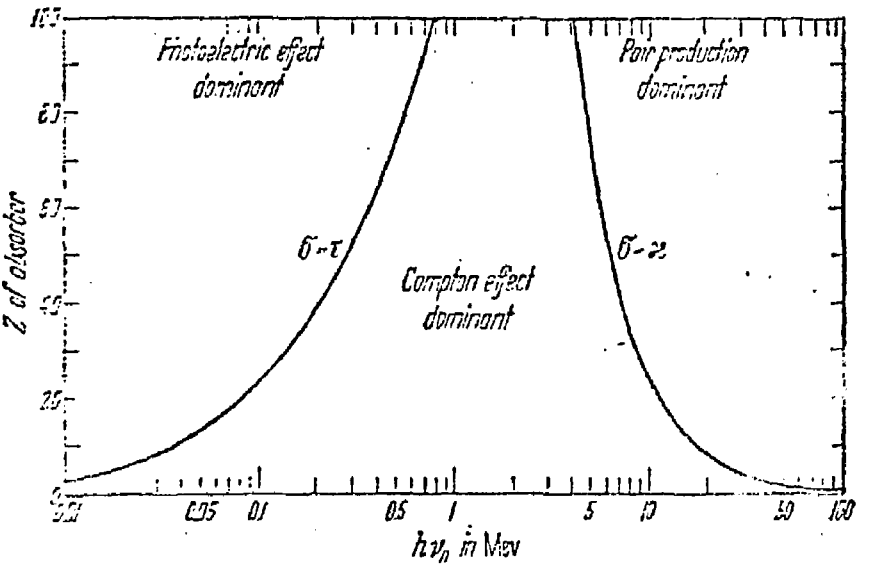
Photoelectric effect dominant
Pair production dominant
Compton effect dominant
σ ~ τ
σ ~ z²
Z of absorber
hν₀ in Mev
0.01
0.05
0.1
0.5
1
5
10
50
100

Fig. 1

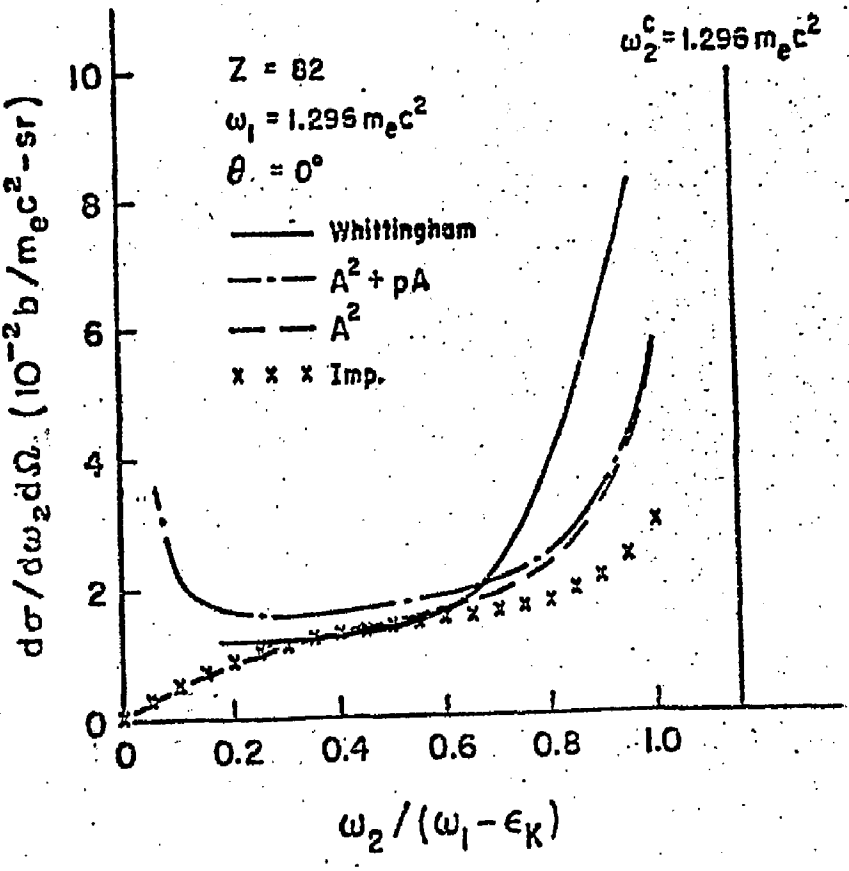
Z = 82
$\omega_1 = 1.296\, m_e c^2$
$\theta = 0°$
Whittingham
$A^2 + pA$
A^2
x x x Imp.
$\omega_2^c = 1.296\, m_e c^2$
$d\sigma/d\omega_2 d\Omega$ $(10^{-2} b/m_e c^2\text{-sr})$
$\omega_2/(\omega_1 - \epsilon_K)$
0
0.2
0.4
0.6
0.8
1.0
2
4
6
8
10

Figure 2

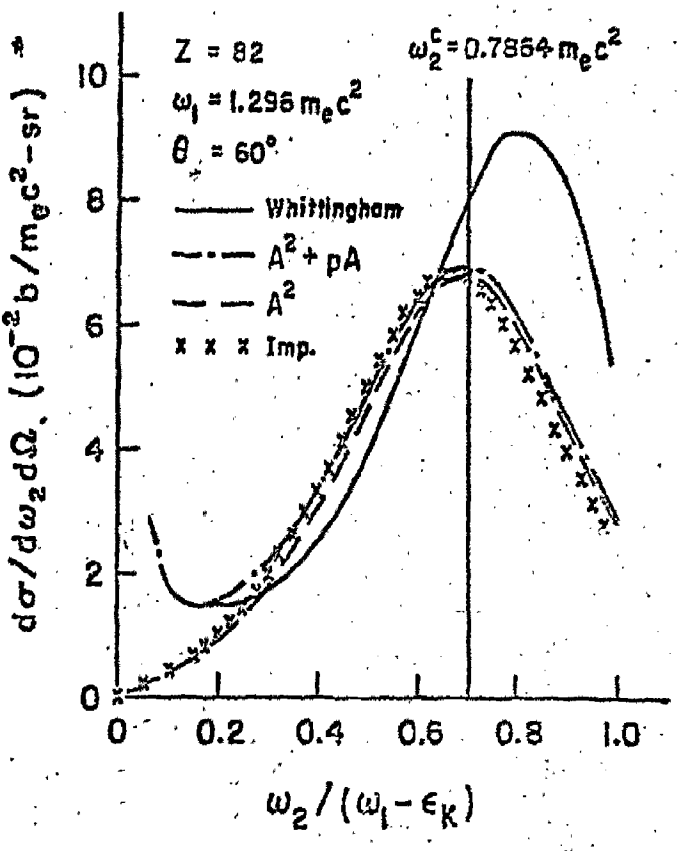
Z = 82
$\omega_1 = 1.296\, m_e c^2$
$\theta = 60°$
$\omega_2^c = 0.7864\, m_e c^2$
Whittingham
$A^2 + pA$
A^2
Imp.
$d\sigma/d\omega_2 d\Omega$, $(10^{-2} b/m_e c^2 - sr)$
$\omega_2/(\omega_1 - \epsilon_K)$
0
2
4
6
8
10
0.2
0.4
0.6
0.8
1.0

Figure 2

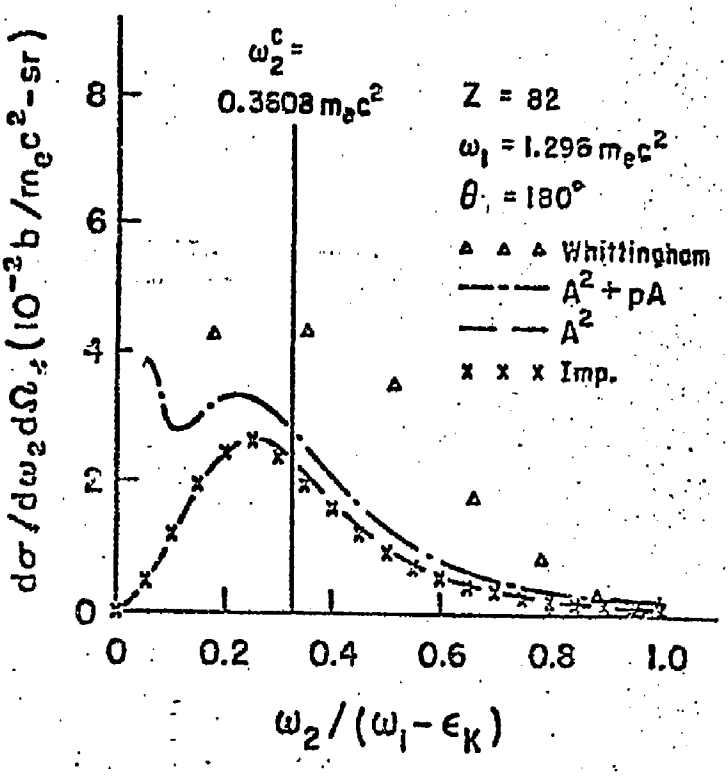
$\omega_2^c =$
$0.3608\, m_e c^2$
$Z = 82$
$\omega_1 = 1.296\, m_e c^2$
$\theta_1 = 180°$
Whittingham
$A^2 + pA$
A^2
Imp.
$d\sigma / d\omega_2 d\Omega_1 (10^{-3} b / m_e c^2 - sr)$
$\omega_2 / (\omega_1 - \epsilon_K)$
0
0.2
0.4
0.6
0.8
1.0
2
4
6
8

Figure 4

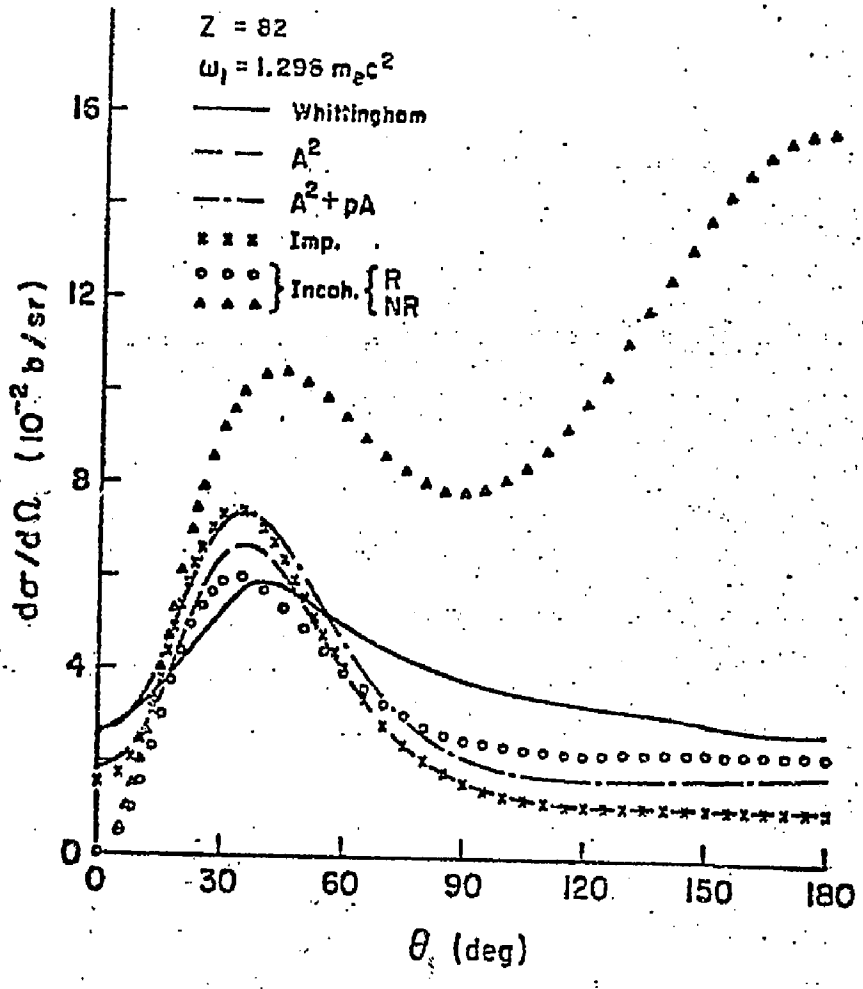
Z = 82
$\omega_1 = 1.296\ m_e c^2$
Whittingham
A^2
$A^2 + pA$
Imp.
Incoh. { R NR
$d\sigma/d\Omega$ (10^{-2} b/sr)
0
4
8
12
16
0
30
60
90
120
150
180
θ_e (deg)

Figure 5